NASA Technical Memorandum 101539

A Wide Bandwidth Electrostatic Field Sensor for Lightning Research

Klaus P. Zaepfel

January 1989

National Aeronautics and
Space Administration

Langley Research Center
Hampton, Virginia 23665

A WIDE BANDWIDTH ELECTROSTATIC FIELD SENSOR FOR LIGHTNING RESEARCH

Klaus P. Zaepfel
NASA Langley Research Center
Hampton, Virginia 23665

ABSTRACT

Data obtained from UHF Radar observation of direct-lightning strikes to the NASA F-106B airplane have indicated that most of the 690 strikes acquired during direct-strike lightning tests were triggered by the aircraft. As an aid in understanding the triggered lightning process, a wide bandwidth electric field measuring system was designed for the F-106B by implementing a clamped-detection signal processing concept originated at the Air Force Cambridge Research Lab in 1953. The detection scheme combines the signals from complementary stator pairs clamped to zero volts at the exact moment when each stator pair is maximally shielded by the rotor, a process that restores the dc level lost by the charge amplifier. The new system was implemented with four shutter-type field mills located at strategic points on the airplane. The bandwidth of the new system was determined in the laboratory to be from dc to over 100k Hz, whereas past designs had upper limits of 10 Hz to 100 Hz. To obtain the undisturbed electric field vector and total aircraft charge, the airborne field mill system is calibrated by using techniques involving results from ground and flight calibrations of the F-106B, laboratory tests of a metallized model, and a finite-difference time-domain electomagnetic computer code.

INTRODUCTION

NASA LANGLEY RESEARCH CENTER has been flying an F-106B delta-wing airplane into thunderstorms to elicit lightning strikes and record the electromagnetic interaction with the aircraft for the purpose of defining the threat to aircraft (1)*. Several additional experiments were also onboard, including four shutter-type field mills for telemetering the electric field conditions of thunderstorms to help identify active cells.

For the research flights before 1985, the frequency range of the electric field measurements onboard the F-106B research airplane was limited to 10 Hz by the rectified, heavily filtered signals obtained from the field mills. However, wide bandwidth electric field measurements were needed by researchers studying aircraft-initiated lightning processes which had been observed by a UHF radar experiment (2). A new system with faster response times was designed and breadboarded, but the development of that design led to the investigation of an unusual design which had been invented many years ago and which held the promise of an exceptionally high frequency response. Both circuit designs, as well as a different electric field sensor (the mill), were eventually incorporated into the flight instrumentation. As can be seen in Fig. 1, both circuit designs share a common preamplifier, but use two different detection schemes. The first employs a synchronous detection scheme used successfully for many years by the Physics Department of New Mexico Institute of Mining and Technology (3), but modified to obtain an update rate of over 200 Hz; while the second, invented by Dr. L. G. Smith of the Air Force Cambridge Research Laboratory and described in 1954, uses the principle of the so-called slow antenna for obtaining frequencies above 200 Hz and zero-clamping for restoring the low-frequency components of the electric field (4). The reference states an upper frequency of 22k Hz. The New Mexico Institute of Mining and Technology design was faithfully copied, but Dr. Smith's design was converted to solid state technology from the original design employing vacuum tubes.

FIELD MILL SYSTEM DESCRIPTION

A field mill system consists of a sensor, a charge amplifier, and a signal detector. The sensor, also referred to as a field mill, consists of several stationary charge collecting plates, referred to as stators, a grounded, rotating shutter, known as the rotor, that shields the stators from, and exposes them to, the electric field which exists at that location, and a motor to drive the rotor. The sensor is installed in the airplane so that the stators are parallel with the skin of the airplane and the rotor is flush with the outside surface of the airplane. Locations of the four sensors on the airplane are shown in Fig. 2. The varying exposure of the stators to the field causes fields of all frequencies to be modulated, including constant fields, with an apparent modulating signal whose peak values are 1 and 0. These conditions are illustrated in Figs. 3 and 4 with simulated stator fields for data frequencies below and above the modulating frequency, respectively. Commonly used dectection schemes recover only frequencies from dc to 10 Hz and filter out the rest. A following section describes a detection scheme that preserves all frequencies up to the cutoff of the electronics.

For greater noise immunity, the charge amplifier is preferably located close to the sensor and is, for this design, placed inside a small preamplifier package along with a gain amplifier. The signal detectors are in a larger enclosure. The aft field mill installation is shown in Figs. 5 and 6. An AC-to-DC converting power supply for the motor is also shown in Fig. 6.

ELECTRIC FIELD SENSOR

An electric field sensor is shown in Fig. 7. The moving parts of the sensor are driven by a dc motor which contains a shaft extending out both ends. The rotor is mounted to one end of the motor shaft and the sync signal shutter, to the other. The rotor is grounded through sliprings on the motor shaft by brushes in the sensor case. The electric field sensor is mounted to the aircraft so that the grounded rotor is approximately flush with the skin, and the rotor end faces outward. The four stator segments are 1 cm below the rotor and insulated from the grounded field mill case by a 1.5 cm thick Kel-F (chlorotrifluoroethylene) slab, a material that has negligible piezo-electric and moisture absorbing properties. The rotor and stators are machined from nonmagnetic stainless steel to minimize effects due to surface charge and contact potential (5). The total geometric stator area is .0035 m^2 of which about half remains uncovered by the two-bladed rotor at any one time. Charge variations (the modulated electric field) are conducted to the charge amplifiers inside the preamplifier package through RG174 cable from threaded rods fastened into the back of the stator plates. RG174 contains non-piezoelectric (polyethylene) dielectric. However, these cables were still somewhat noise-generating, and will be replaced this season by low-noise cables of a type that, in bench tests, produced only half the vibration induced noise of the RG174.

The optical switches are mounted to the shutter cover, which is adjustable for aligning the phase between sync pulse and signal peak (or zero). The switch is a commercially made unit that contains an infrared photodiode opposite a gap from a phototransistor. Whenever the passage of a shutter blade interrupts the beam, the transistor is switched off.

CLAMPED DETECTION

This method of demodulation is capable of passing frequencies from dc to the limits imposed by the parasitic capacitance in the circuits. The method takes advantage of the exposed stator area acting as a so-called slow antenna. Consequently, the signals leaving the charge amplifiers contain information covering the bandpass of the charge amplifiers.

When Dr. L. G. Smith developed his detection circuitry, he also developed a field mill design that minimized fringing by having the rotor in close proximity to the stators, thereby producing triangular-wave modulation. The changing charge (q) on the stators as they were alternately being exposed to, and shielded from, the E-field was linearly related to the exposed stator area (A) by $q = \varepsilon_0 AE$. The two signals complemented each other because as one signal decreased, the other increased at the same rate. The triangular wave was composed of the

* Numbers in parentheses designate references at end of paper.

dc and the ac components which increased and decreased in amplitude at the same time. By adding the two waves, the signals were restored to full amplitude.

Because close rotor-stator spacing causes water-shorting during thunderstorm penetrations, a wide spacing of approximately 1 cm was selected for the F-1068 design. The resulting fringing produces sinusoidal modulation instead of the previously described triangular wave modulation, and sinusoidal modulation is used in the following explanation of this detection method.

If the field impinging on the stators of the field mill could be measured directly, it would look like a sinusoid with a frequency of twice the rotor revolution per second and peaks bounded between zero (stator covered by rotor) and instantaneous field strength (stator uncovered by rotor). Examples of simulated stator signals are shown in Figs. 8(a) and 8(b). These signals can be described mathematically by

$$1/2(1 + \sin \omega_c t)E(t) \qquad (1)$$

and, because the other stator is modulated with a 180-degree phase delay, the other signal can be described by

$$1/2(1 - \sin \omega_c t)E(t) \qquad (2)$$

for a two-stator pair geometry such as this one. The field strength, E(t), could be recovered completely if the two outputs could be added. However, the charge amplifier in each channel requires a bleed-off resistor that blocks any dc components; in effect, the 1/2E(t) component in both of the above equations is lost. This component can be periodically restored by introducing a circuit that clamps the signal to zero volts each time the stator is maximally covered by the rotor. Fig. 9 is a block diagram of a detection technique that does just that, and Fig. 10 shows the following steps in the processing of a signal containing both a dc and an ac component:

(a) The signals at the detector inputs without any dc component;

(b) the clamping pulses synchronized to the rotor position;

(c) the data signals after zero-clamping;

(d) the restored signal with both dc and ac components.

Fig. 11 is a simplified schematic of the detector without the charge amplifier. The outputs from the preamplifier, which contains the charge amplifiers, are ac-coupled through C1 and C2 to the CMOS clamping switches. Whenever the stator is completely shielded by the rotor, the appropriate switch closes, thereby momentarily forcing the signal to ground. Resistors R1 and R2, together with C1 and C2 provide a long time constant, which maintains the offset until the next switch closure. Voltage followers A1 and A2 provide the high impedance isolation from the summing stage at operational amplifier A3. Limited gain adjustment is provided by R3 and R4 to ensure that the two signals are truly complementary. Output resistor R5 provides A3 with cable isolation to prevent spurious oscillation. Nevertheless, a buffer amplifier (not shown) was required at this output, as well as at the other outputs, to drive the long cable runs to the data recording system. Fig. 12 shows the detector output for each of the simulated inputs of Fig. 8.

SYNCHRONOUS DETECTION

The electrical signals derived from the modulated electric field are sampled separately at all positive and negative peaks, and held until the next sample is obtained, as shown in Fig. 13. The timing of the sampling is controlled by synchronizer signals derived from optical switches that sense a chopper wheel driven by the same motor that turns the rotor. Phasing is such that, when a stator pair is fully exposed or fully covered, a sync pulse is generated which samples the signal at positive and negative peaks. A peak value of one polarity is sampled and held, replacing the old peak being held in the sample-and-hold (S & H) circuit, and differenced with the peak values (obtained 180 electrical degrees earlier) being held in the S & H circuit assigned to the opposite polarity. Peak-to-peak values are obtained in this manner for both stator pairs, and these values are added to obtain the detector output. This occurs twice per motor revolution for each stator pair. The summed output is unfiltered to assure "immediate" response of the system to field changes.

A more detailed diagram is shown in Fig. 14. CMOS switches S3 and S4, controlled by the sync signals derived from the rotor-coupled optical switches, alternately sample the modulated signal from one of the stator pairs at positive and negative peaks at the same time that S5 and S6 sample the other stator pair at negative and positive peaks. Capacitors C3 through C6 hold the sampled values between switch closures. A guard ring around each hold line is driven by the line's signal to minimize leakage from the holding capacitor. Voltage followers A4 through A7 provide this drive as well as isolation of the capacitors from the following stages. The peak-to-peak value of each stator signal is derived by A8 and A9, and the sum of these two values is obtained by A10.

THE SYNCHRONIZER PULSE

Two pulse trains time the operation of both detection circuits. They are in synchronism with the rotor and each consists of two equally-spaced pulses per rotor revolution. The two pulses in the second pulse train are displaced from the first by 1/4 revolution. The synchronous detection circuit uses both pulse trains to sample the stator signals when each stator pair is completely uncovered and again when the pair is completely covered for a sample at each peak. The clamped detection circuit uses both pulse trains to clamp the signals to ground only when each stator pair is completely covered. The pulse signal labeled CLAMP A is identical to SYNC B, and vice versa.

The two pulse trains are generated by several circuits shown in Fig. 15 that shape signals which originate in two interrupter-type optical switches mounted radially on the field mill body 90 degrees apart. A mechanical chopper, which consists of two lobes and is fastened to the motor shaft, triggers each switch twice per revolution. The biasing networks on the phototransistors in the optical switches and circuits A11 through A14 are designed to generate square-waves with fast rise and fall times. The outputs of the optical switches are isolated from the square-wave generators, A13 and A14, by voltage followers, A11 and A12. Unipolar, TTL-compatible waveforms, from which one-shots M1 and M2 generate the sync pulses, are created by D1, D2, and R6 through R9.

OUTPUT FILTER

The output from the synchronous demodulation circuit is stepwise responsive. In order to have the capability of presenting a more conventionally appearing signal, although of slower response, a 10-Hz, fourth-order, low-pass active filter was included in the system. If the field mill system can be made sufficiently noise-immune for fair-weather field measurements, this filter will be used at 10 Hz or 1 Hz cutoff (Fig. 16) to further quiet the signals during calibration flights (6).

FREQUENCY RESPONSE

Two independent circuits were designed to detect the field information contained in the pre-amplifier outputs. They have been described in detail, above. No frequency response curves were obtained for the synchronous detection circuit, although, if filtered, about 20 Hz to 30 Hz could be attained. Unfiltered as it is, update rates are about 250 samples per second. However, data frequencies above that rate are aliased and incorrectly represented as lower frequencies.

Obtaining the frequency response characteristics in the laboratory was difficult because an alternating field large enough to overcome the noise floor of the electronics and of the lab environment was unavailable. An estimate of the frequency response characteristics was obtained for the clamped detection technique by three methods: simulated sensor signal, and actual sinusoidal fields applied to a sensor with rotating and non-rotating rotor.

Large signals were simulated by a circuit which produced the signal described by equations 1 and 2 above. This simulator is capable of generating signals that represent constant fields, alternating fields, or a combination of the two. It is described in a later section. To obtain actual sinusoidal fields, amplified sinusoidal signals were applied to a flat plate mounted 3 mm from the rotor, and the gain of the field mill electronics was increased to compensate for the low signal levels.

The results of these calibrations are plotted in Fig. 17 and show a bandwidth of over 100k Hz. While the characteristics resulting from the simulated inputs are flat down to dc as expected, those for the case with a running rotor are 2 dB down below 100 Hz. At this time no explanation is available for this phenomenon. Of additional interest is the case of the stationary rotor. It demonstrates the field mill system's ability to function as a slow antenna as indicated previously.

CALIBRATION

Two electric field regions of interest on, or about, the research aircraft are the local fields at the sensor locations and the ambient fields far enough from the aircraft to be undisturbed by it. The local fields are expected to be different from the ambient fields because the aircraft carries charge and its shape distorts the ambient field in amplitude and direction by amounts defined by a matrix of enhancement coefficients (form factors). Therefore, each region requires a different calibration procedure. Local fields will be calibrated in-place on the airplane by applying a known field with a high-voltage plate mounted parallel to the face of each sensor. This procedure also serves as a pre-flight check of the systems.

The enhancement coefficients a_{ij} (the form factors) of the set of simultaneous equations are shown below in terms of ambient fields, F, aircraft charge, Q, and local fields, E. The F-coordinate system is that of the aircraft (Fig. 2): x is nose to tail; y is right to left wing tips; z is top to bottom. Field mill locations (Fig. 2) are designated by local fields, E_A, E_L, E_R, E_F located aft, left, right, and forward, respectively, on the airplane.

$$\begin{aligned} E_A &= a_{11}F_x + a_{12}F_y + a_{13}F_z + a_{14}Q \\ E_L &= a_{21}F_x + a_{22}F_y + a_{23}F_z + a_{24}Q \\ E_R &= a_{31}F_x + a_{32}F_y + a_{33}F_z + a_{34}Q \\ E_F &= a_{41}F_x + a_{42}F_y + a_{43}F_z + a_{44}Q \end{aligned} \qquad (3)$$

To reduce the number of unknowns and calibration flight attitudes, we take advantage of aircraft symmetries at the Y-field mill locations. Fields that impinge on the face of sensors E_L and E_R in the same direction have coefficients of the same sign (a_{21}, a_{31} for F_x; a_{23}, a_{33} for F_z; a_{24}, a_{34} for Q). Fields that impinge on E_L and E_R in opposite directions have coefficients of opposite sign (a_{22}, a_{32} for F_y). The field, F_y, has no net effect on E_F because E_F is located on the aircraft centerline: as many F_y field lines enter as leave the surface ($a_{42} = 0$ for F_y). Applying these conditions, the coefficients can be redefined as follows:

$$\begin{aligned} a_{21} &= a_{31} = a_2 \\ a_{22} &= -a_{32} = b_2 \\ a_{23} &= a_{33} = c_2 \\ a_{24} &= a_{34} = d_2 \\ a_{42} &= 0 \end{aligned}$$

When these and other redefined coefficients are substituted into the above equations, the following enhancement coefficient matrix can be written:

$$\begin{matrix} a_1 & b_1 & c_1 & d_1 \\ a_2 & b_2 & c_2 & d_2 \\ a_2 & -b_2 & c_2 & d_2 \\ a_3 & & c_3 & d_3 \end{matrix} \qquad (4)$$

On the one hand, the immediate consequence of this symmetry is that, if left and right field mill outputs are subtracted, their difference is proportional purely to F_y. On the other hand, their sum is a function not only of Q, but also of F_x and F_z.

To obtain the enhancement coefficient matrix, three independent calibration schemes are being considered. Although a direct calibration of the airplane is preferred, the results of all three will establish the degree of confidence (and perhaps, of error) that can be placed on the resulting calibration. They are inflight calibration, scale model calibration, and computer model calibration.

IN-FLIGHT CALIBRATION--Because the data system is not accessible during flight, the field mill electronics are preset, and data from each field mill channel is recorded individually. The airplane is flown in a vertical ambient field at various attitudes at a safe altitude so that it receives inputs from other directions that cause field vectors to go to zero or to cancel each other. It is also flown level in a vertical field of known magnitude provided by a reference field mill located on the ground or borne aloft by a tethered balloon, thereby producing data that calibrates the z-directed field (with respect to the aircraft axis). From this data, a systematic selection of data for specific airplane attitudes which force undesired ambient field components in the above equations to zero, allows an in-house developed computer program to calculate the enhancement coefficients. This program is equivalent to a process described in detail by Kasemir (7) for an airborne analog computer which contains adders and subtracters with weighting factors, P, which had to be adjusted during appropriate maneuvers in flight. A block diagram equivalent of the program to be used for the F-106B airplane is shown in Fig. 18. Each weighting factor can be calculated because equations derived from the enhancement coefficient matrix (equation 4) are greatly simplified by the appropriate airplane attitudes. Because each field mill output is a function of the three ambient field components and total aircraft charge (F_x, F_y, F_z, Q) as described by equation 3, the program has to isolate the variables, F's and Q, and then scale them from the recording system to the reference vertical field. In Fig. 18 each adder-subtracter output, U, represents a step in this isolation process. The outputs U1, U3, and U4 are no longer functions of one or more of these variables, and each of the outputs U6, U7, and U8 is no longer a function of any but the desired, unscaled variable. Weighting factors P10 through P13 provide the proper engineering-units scaling. The program was checked by calculating the local fields during a simulated calibration flight. A vertical ambient field was assumed, and the local fields were derived using enhancement coefficients obtained by Electromagnetic Applications (EMA), Inc., of Denver, Colorado from their finite-difference 3-D computer model of the F-106B. These local fields were then substituted into the in-house computer program to derive enhancement coefficients, which reproduced EMA's coefficients exactly. The values of the P's are listed in Table I. However, because most of the P's are calculated by using P's that have been calculated during previous steps, an initial measurement error incurred in a real situation may be cumulative. Another major drawback to this calibration method is that the charge distribution coefficients, d, cannot be obtained; although the effects of charge on the ambient field components can be eliminated, and a data channel that is proportional only to charge can be derived, no absolute calibration can be obtained. In lieu of feasible direct methods to obtain the d coefficients through in-flight tests, several alternate methods are being pursued.

MODEL CALIBRATIONS--These efforts will determine the d's through comparison of results from scale model laboratory tests, from full-scale ground tests over a uniform ground plane with analytical removal of ground plane effects, and from purely analytical calculation of the d's. The scale model tests to be performed by EMA, Inc., involve the high voltage charging of a metalized F-106 scale model and measuring the charge at the field mill locations. This technique will also be used to determine the other field enhancement coefficients by immersing the scale model in a uniform electric field in three orthogonal orientations. The full-scale ground tests involve charging the aircraft while it is parked on a uniform metal wire grid ground plane, determining charge from voltage and capacitance of the aircraft, and concurrently recording the field mill outputs. Ground plane effects will subsequently be removed analytically using the 3-D computer code. Results from the above laboratory, full scale, and analytical approaches will be combined to arrive at a best estimate of the d coefficients.

FLIGHT DATA

Although the field mill data system was onboard the F-106B for the duration of the 1985 thunderstorm season, circumstances never permitted it to be calibrated for ambient fields. Hence, the data that are shown are from field mill outputs at, or about, the time of reported strikes. Fig. 19 shows the output of the right field mill for three examples of lightning attachments to the airplane. For each example, the top trace is the output from the zero-clamped detector recorded on an FM data channel with a frequency response of 0 Hz to 10000 Hz and a modulation index of 2.2. The bottom trace is the output from the synchronous detector recorded on an FM channel with a response of 0 Hz to 250 Hz and a modulation index of 4. Before and after the strikes, all three examples show a much better definition of the electric field structure in time and amplitude for data from the zero-clamped detector than from the synchronous detector.

At times, however, data is highly suspect, probably degraded by the thunderstorm environment. Causes are still speculative but two possibilities may be that the stators are at times shorted by rain or shielded by corona or that the charge amplifier is driven into saturation by nearby lightning. Portions of Fig. 19(b) and 19(c) show unrealistic behavior during and for some time after a strike. Either saturation of the charge amplifier because of an extremely large concentration of charge at the field mill sensor or attenuation of the signal due to corona or rain are possible causes. The appearances of fairly pure sinusoidal signals of approximately 200 Hz in the zero-clamped detector output of Fig. 19(b) and (c) indicate that one input to the summing circuit recovers slightly faster than the other.

SIMULATOR

A field mill simulator was designed and built to generate a signal large enough to permit obtaining frequency response characteristics of the electronic portion of the field mill system. The device uses the inputs from a low-frequency signal generator with a dc offset feature for data inputs, $f_D(t)$, and a variable-phase function generator for the rotor modulation and the sync signal inputs. Two multipliers with differential inputs and adders configured as shown in Fig. 20 provide the desired functions of equations 1 and 2, with $f_D(t)$ simulating E(t). The differential inputs permit the modulation function, sin $\omega_c t$, to be inverted to produce the required minus sign. A square wave output from the variable-phase generator that is the same frequency as the rotor modulation provides the sync signal normally produced by the photo-optical switches mounted in the field mill sensor.

SUMMARY

An airborne electric field measurement system which combines frequency characteristics of a shutter-type field mill system and a flat-plate dipole (slow antenna) system has been developed and demonstrated during thunderstorm penetrations on the F-106B research airplane. A comparison of simultaneous flight data records obtained from the zero-clamped detector and from the more conventional synchronous detector showed the superior temporal resolution of the former system while preserving the low frequencies of the latter.

The data also showed shortcomings of making ambient field measurements in thunderstorms, including momentary signal losses or distortions. Fortunately, most problem areas in the data are easily recognizable, and data thus affected should be ignored.

Although a system calibration was never achieved, several procedures have been developed and will be performed during the 1986 season.

Table I - Values of Weighting Factors, P, for 3-D Code Model of F-106B

P1	5.948
P2	26.96
P3	1.837
P4	1.290
P5	.05137
P6	.04220
P7	0.5137
P8	.01036
P9	15.37
P10	7.945
P11	.3425
P12	.01789
P13	.001812

REFERENCES

1. Pitts, F. L., "Electromagnetic Measurement of Lightning Strikes to Aircraft,"AIAA Journal of Aircraft, Vol. 19, No. 3, March 1982, pp. 246-250.

2. V. Mazur, B. D. Fisher, J. C. Gerlach, "Lightning Strikes to an Airplane in a Thunderstorm," AIAA Journal of Aircraft, Vol. 21, No. 8, August 1984, pp. 607-611. Supercedes AIAA-84-0468.

3. Winn, W. P., personal communications, October 1983.

4. L. G. Smith, "An Electric Field Meter With Extended Frequency Range," The Review of Scientific Instruments, Vol. 25, No. 5, May 1954, pp. 510-513.

5. J. C. Willett, J. C. Bailey, "Contact Potential and Surface Charge Effects in Atmospheric Electrical Instrumentation," NRL Memorandum Report 5063, Naval Research Laboratory, Washington DC, April 26, 1983.

6. Circuit design from National Semiconductor Linear Databook, 1980, p. 3-36.

7. H. W. Kasemir, "Electric Field Measurements from Airplanes," Fourth Symposium on Meteorological Observations and Instrumentation, April 1978, pp. 506-513.

8. V. Mazur, L. H. Ruhnke, T. Rudolph, "Effect of E-Field Mill Location on Accuracy of Electric Field Measurements With Instrumented Airplane," International Conference on Lightning and Static Electricity, June 1986.

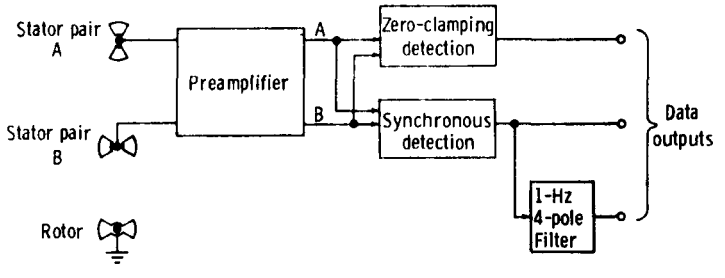

Fig. 1 - F-106B field mill system block diagram

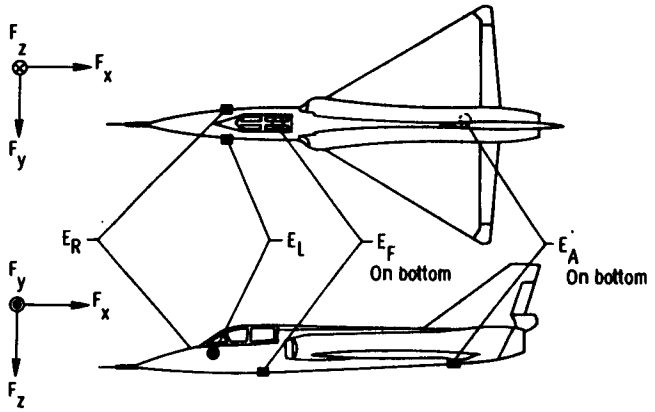

Fig. 2 - Field mill locations on F-106B research airplane and field sign conventions

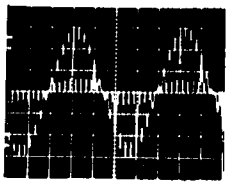

Fig. 3 - Simulated low-frequency stator field

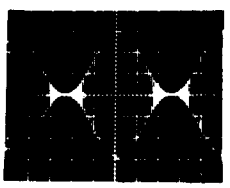

Fig. 4 - Simulated high-frequency stator field

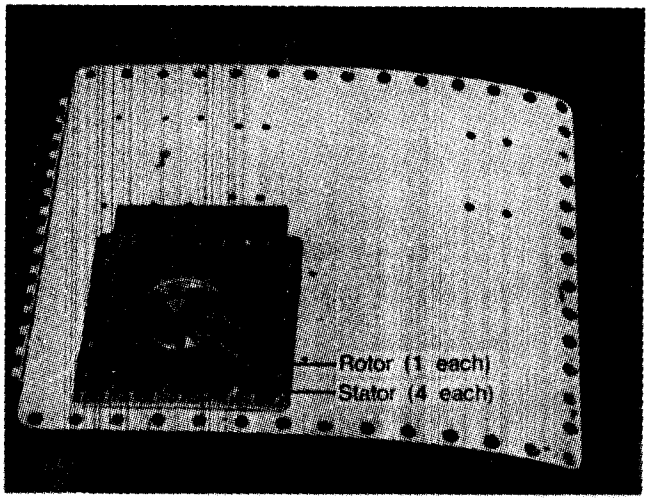

Fig. 5 - Field mill installation in F-106B access door (exterior)

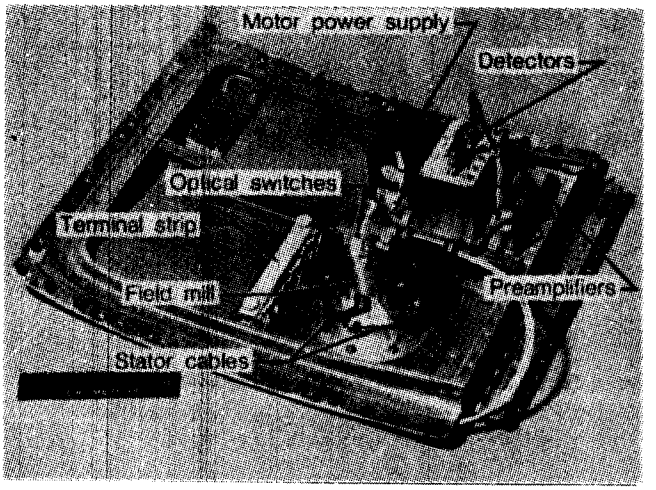

Fig. 6 - Field mill installation in F-106B access door (interior)

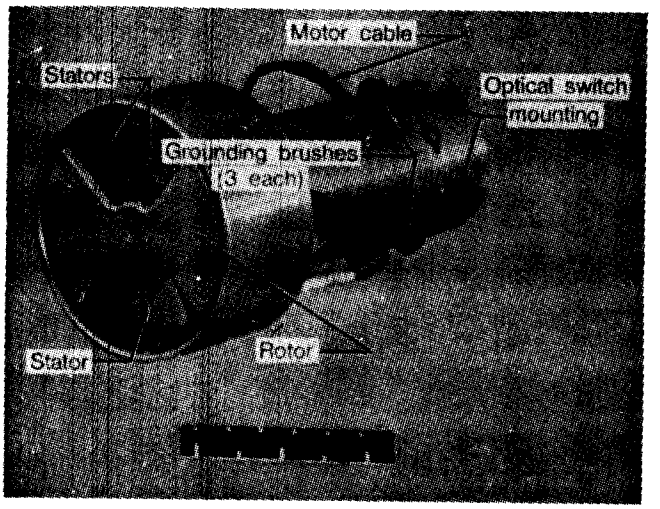

Fig. 7 - Electric field sensor

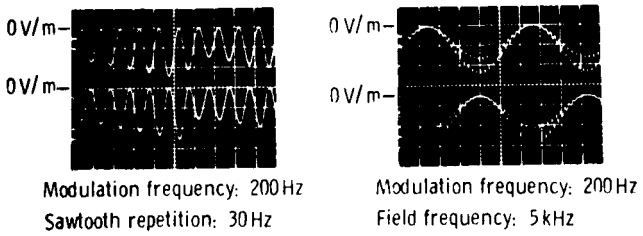

Fig. 8 - Examples of stator signals (simulated)

(a) - Sawtooth field with constant offset

(b) - Sinusoidal field with constant offset

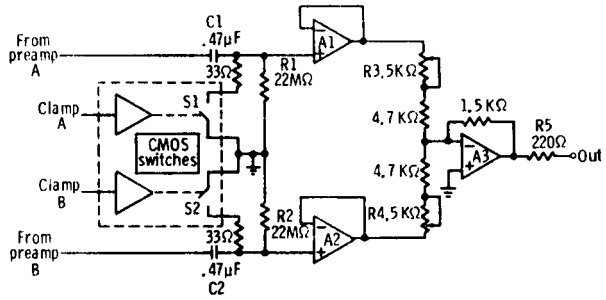

Fig. 11 - Clamped detector circuit diagram (simplified)

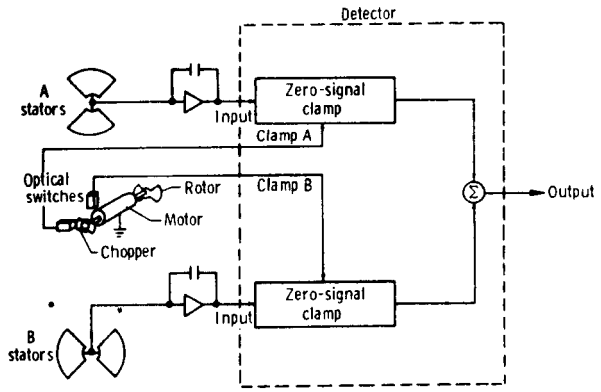

Fig. 9 - Clamped detection block diagram

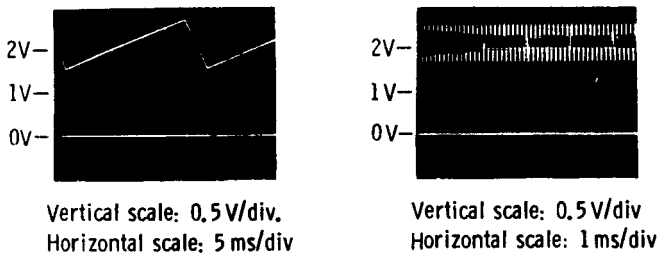

Fig. 12 - Clamped detector outputs resulting from inputs of Fig. 8

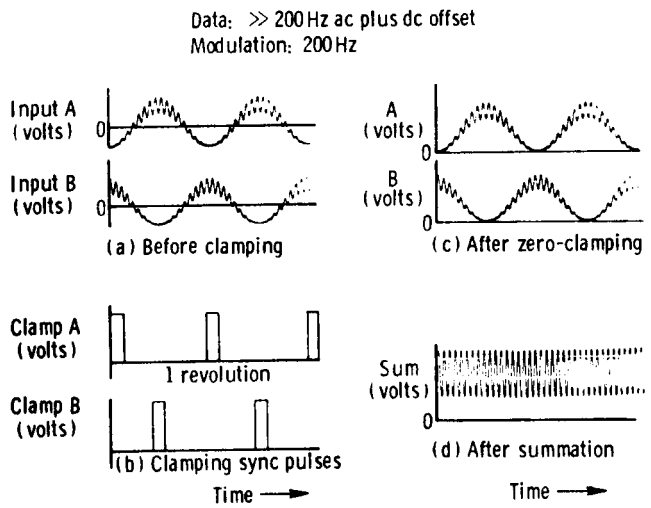

Fig. 10 - Clamped detection

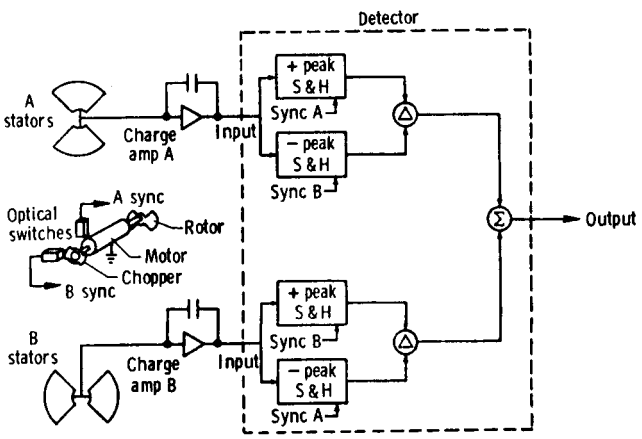

Fig. 13 - Synchronous detection block diagram

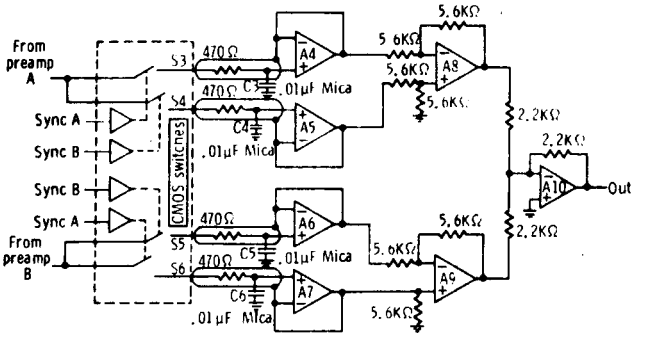

Fig. 14 - Synchronous detector circuit diagram (simplified)

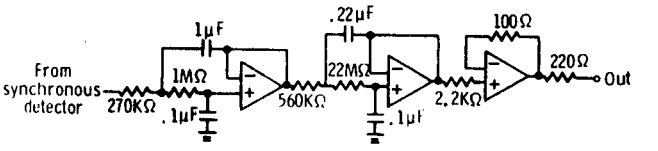

Fig. 16 - 1-Hz, 4th order, low-pass filter

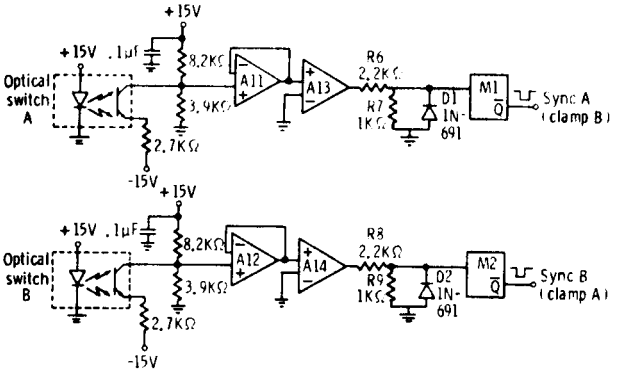

Fig. 15 - Synchronizer pulse generator circuit diagram (simplified)

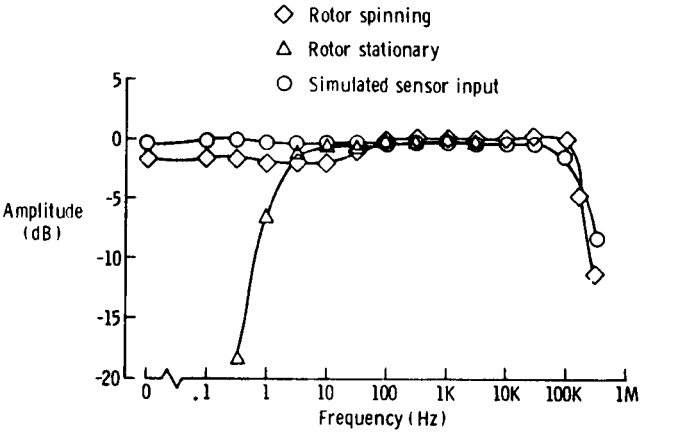

Fig. 17 - Frequency calibrations

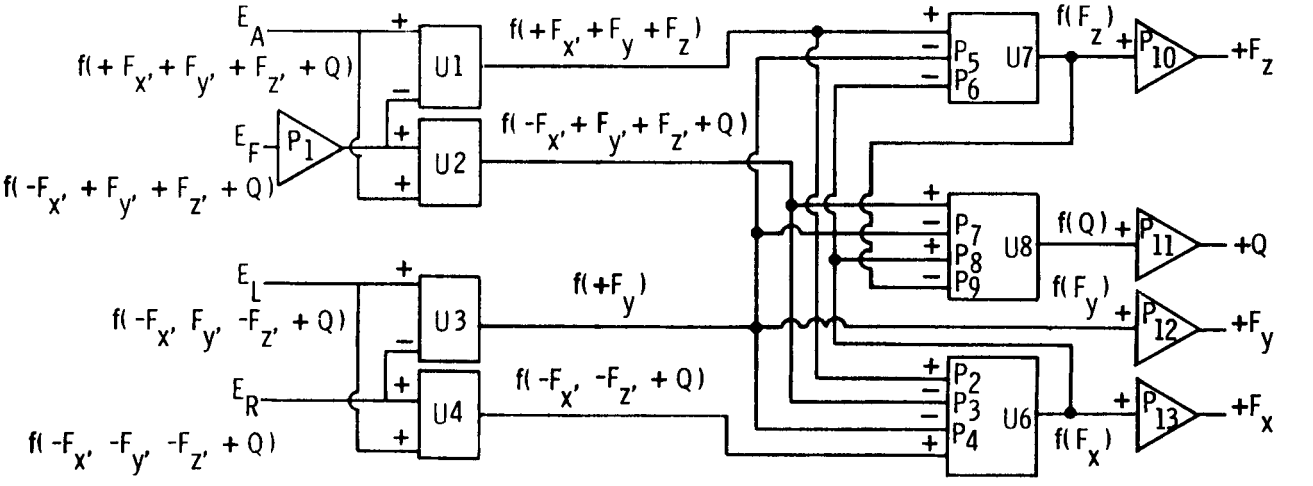

Fig. 18 - Block diagram representation of computer code for inflight calibrations

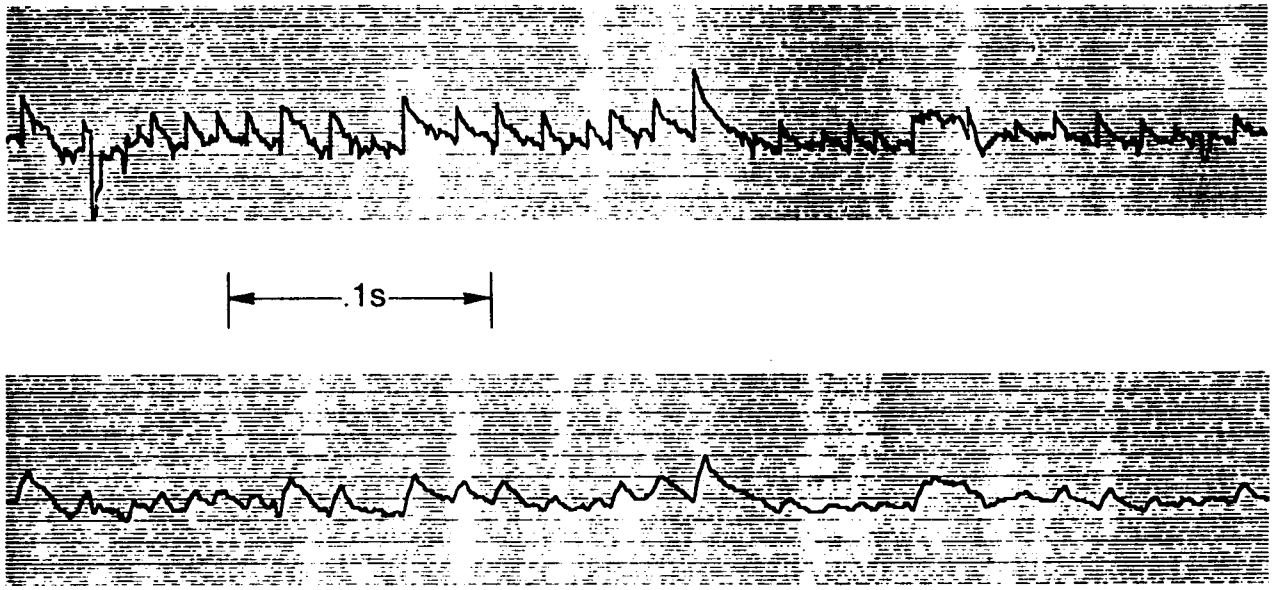

(a) Flight 85-033, 22:26:15 UT

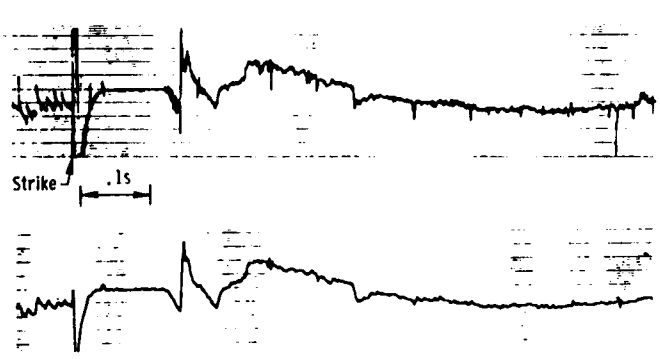

(b) Flight 85-033, 22:23:29 UT

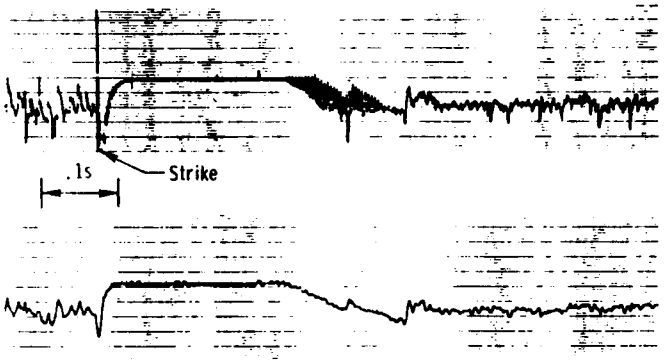

(c) Flight 85-033, 22:26:15 UT

Fig. 19 - Comparisons of E_R field mill system outputs: clamped detection (top); synchronous detection (bottom)

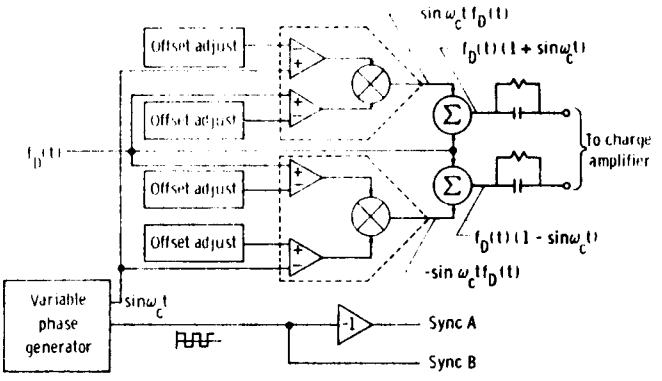

Fig. 20 - Simplified schematic of electric field sensor simulator

NASA
National Aeronautics and Space Administration

Report Documentation Page

1. Report No.	2. Government Accession No.	3. Recipient's Catalog No.
NASA TM-101539		

4. Title and Subtitle	5. Report Date
A Wide Bandwidth Electrostatic Field Sensor for Lightning Research	January 1989
	6. Performing Organization Code

7. Author(s)	8. Performing Organization Report No.
Klaus P. Zaepfel	
	10. Work Unit No.
	505-66-21-04

9. Performing Organization Name and Address	11. Contract or Grant No.
NASA Langley Research Center Hampton, VA 23665-5225	
	13. Type of Report and Period Covered
	Technical Memorandum

12. Sponsoring Agency Name and Address	14. Sponsoring Agency Code
National Aeronautics and Space Administration Washington, DC 20546-0001	

15. Supplementary Notes

Presented at the 1986 Conference on Lightning and Static Electricity, Dayton, OH, June 24-26, 1986.

16. Abstract

Data obtained from UHF Radar observation of direct-lightning strikes to the NASA F-106B airplane have indicated that most of the 690 strikes acquired during direct-strike lightning tests were triggered by the aircraft. As an aid in understanding the triggered lightning process a wide bandwidth electric field measuring system was designed for the F-106B by implementing a clamped-detection signal processing concept originated at the Air Force Cambridge Research Lab in 1953. The detection scheme combines the signals from complementary stator pairs clamped to zero volts at the exact moment when each stator pair is maximally shielded by the rotor, a process that restores the dc level lot by the charge amplifier. The new system was implemented with four shutter-type field mills located at strategic points on the airplane. The bandwidth of the new system was determined in the laboratory to be from dc to over 100k Hz, whereas past designs had upper limits of 10 Hz to 100 Hz. To obtain the undisturbed electric field vector and total aircraft charge, the airborne field mill system is calibrated by using techniques involving results from ground and flight calibrations of the F-106B, laboratory tests of a metallized model, and a finite-difference time-domain electromagnetic computer code.

17. Key Words (Suggested by Author(s))	18. Distribution Statement
Lightning Electric Field Measurements Field Mills (Wide Band) Thunderstorn Measurements	Unclassified-Unlimited Subject Category 47

19. Security Classif. (of this report)	20. Security Classif. (of this page)	21. No. of pages	22. Price
Unclassified	Unclassified	11	A03